Intermolecular Interactions of Xe Atoms Confined in One-dimensional Nanochannels of Tris(*o*-phenylenedioxy)cyclotriphosphazene as Studied by High-pressure ^{129}Xe NMR

Hirokazu Kobayashi[a], Takahiro Ueda[a,b], Keisuke Miyakubo[a], and Taro Eguchi[a,b]

[a] Department of Chemistry, Graduate School of Science, Osaka University, Toyonaka, Osaka 560-0043, Japan
[b] The Museum of Osaka University, Osaka University, Toyonaka, Osaka 560-0043, Japan

Reprint requests to Prof. T. E.; E-mail to:eguchi@museum.osaka-u.ac.jp

Z. Naturforsch. **58a,** 727 – 734 (2003); received September 9, 2003

The pressure dependence of the ^{129}Xe chemical shift tensor confined in the Tris(*o*-phenylenedioxy) cyclotriphosphazene (TPP) nanochannel was investigated by high-pressure ^{129}Xe NMR spectroscopy. The observed ^{129}Xe spectrum in the one-dimensional TPP nanochannel (0.45 nm in diameter) exhibits a powder pattern broadened by an axially symmetric chemical shift tensor. As the pressure increases from 0.02 to 7.0 MPa, a deshielding of 90 ppm is observed for the perpendicular component of the chemical shift tensor $\delta_\perp$, whereas a deshielding of about 30 ppm is observed for the parallel one, $\delta_\parallel$. This suggests that the components of the chemical shift tensor, $\delta_\parallel$ and $\delta_\perp$, are mainly dominated by the Xe-wall and Xe-Xe interaction, respectively. Furthermore, the effect of helium, which is present along with xenon gas, on the ^{129}Xe chemical shift is examined in detail. The average distance between the Xe atoms in the nanochannel is estimated to be 0.54 nm. This was found by using $\delta_\perp$ at the saturated pressure of xenon, and comparing the increment of the chemical shift value in $\delta_\perp$ to that of a β-phenol/Xe compound.

Key words: High-pressure ^{129}Xe NMR; TPP; One-dimensional Nanochannel; Pressure Dependence; ^{129}Xe Chemical Shift Tensor.

1. Introduction

Xenon-129 NMR spectroscopy is known to be one of the most powerful and useful tools to study the porosity and local structure of porous materials [1 – 9]. Xenon has a van der Waals diameter of 0.432 nm, comparable in size to that of methane. The atomic diameter of xenon enables it to penetrate almost any porous material [4]. The ^{129}Xe isotropic chemical shift for atomic xenon varies over more than 300 ppm depending on the physical and chemical environment of the xenon atoms. The ^{129}Xe chemical shift in restricted space is very sensitive to the size and shape of the cavity. Therefore ^{129}Xe NMR has been extensively applied to investigate the local environment of xenon in pores as well as to characterize the porosity of numerous systems [7 – 15].

In the past decade, hyperpolarized (HP) xenon, generated by the optical pumping of Xe (g) in the presence of Rb (g) with 795 nm laser irradiation, has been applied to enhance the sensitivity of ^{129}Xe NMR [16, 17]. As a result of the ^{129}Xe nuclear spins becoming polarized through hyperfine coupling to the unpaired polarized electron spins of Rb atoms, the polarization of Xe nuclear spins is enhanced up to 5% or more. Thus, HP xenon makes it possible to study the nanochannels and surfaces with high sensitivity [18 – 25]. On the other hand, Nagasaka et al. have developed a high-pressure ^{129}Xe NMR technique with a conventional *in situ* variable pressure NMR probe, allowing studies with pressures up to 20 MPa [11]. This technique has been used to characterize the free volumes of synthetic polymers with high equilibrium pressure [11]. It has also been used to investigate the pore size and local structure around the xenon atoms confined in dehydrated (±)-[Co(en)$_3$]Cl$_3$ [15]. In our previous studies we have clarified that Xe confined in a dehydrated (±)-[Co(en)$_3$]Cl$_3$ crystal exhibits an axially symmetric chemical shift tensor [15]. Furthermore, it is found that $\delta_\perp$ increases with increase in pressure of xenon gas, whereas $\delta_\parallel$ is almost independent of pressure, implying that $\delta_\perp$ depends mainly on the xenon density,

whereas $\delta_{\|}$ is principally independent of the xenon density. Thus, the chemical shift tensor of ^{129}Xe confined in the nanochannel provides us with useful information about the pore symmetry as well as the Xe-Xe and Xe-wall interactions. However, the observation of chemical shift anisotropy (CSA) for Xe atoms confined in the nanochannel has only been reported in a few systems [15, 26 – 28].

Tris(*o*-phenylenedioxy) cyclotriphosphazene (TPP) is one of the compounds in which confined xenon exhibits the powder pattern broadened by the chemical shift tensor. TPP has a metastable one-dimensional nanochannel whose diameter is a little larger than that of a xenon atom (0.45 nm). TPP is a family of cyclophosphazenes, and is recognized as one of the first organic zeolites [29 – 31]. TPP is soluble in most organic solvents and crystallization of TPP results in inclusion compounds (ICs) with solvent molecules. The inclusion compound with benzene is the most common. Above 423 K, the pseudo-hexagonal lattice transforms into a monoclinic lattice. Heating at 348 K for a few hours can remove the benzene from the TPP host channels and results in a solvent free metastable crystal which has a pseudo-hexagonal lattice and is stable up to 423 K [32]. The benzene ICs are crystallized in a crystal lattice with a space group of $P6_3/m$ and contain two formula units in the unit cell. The lattice parameters are a = 1.171 nm and c = 1.003 nm. The lattice parameters of TPP depend on the recrystallization solvents, whereas their space group remains $P6_3/m$ [29, 33].

For TPP ICs, the dynamics of several guests such as perdeutrated benzene, cyclopentane or mesitylene was studied by ^{2}H NMR [34 – 35]. In TPP/Benzene ICs, benzene molecules undergo molecular reorientation around the C_6 axis lying along the channel axis. Commoti et al. studied the characterization of the local structure and polymorphism of the TPP host molecule by solid state ^{13}C and ^{31}P MAS NMR and differential scanning calorimetry (DSC) [32]. They studied the dynamic behavior of TPP molecules as well as guest molecules through the ^{13}C spin-lattice relaxation time (T_1) at room temperature. They found that TPP undergoes librations in the phenylenedioxy group with a large amplitude similar to that of the paddling motion in both TPP/benzene IC and guest-free TPP. Furthermore, the chemical shift of ^{129}Xe confined in TPP one-dimensional nanochannels using continuous-flow HP ^{129}Xe NMR technique was reported by Sozzani et al. [26] and Meersmann et al. [27]. The former examined ^{129}Xe adsorbed into TPP nanochannels. The ^{129}Xe NMR spectrum exhibits anisotropic signals broadened by the chemical shift anisotropy and depends strongly on the Xe loading [26]. The latter examined the single-file diffusion behavior of xenon in the TPP one-dimensional nanochannel using continuous-flow optical pumping ^{129}Xe NMR spectroscopy [27]. They clarified that single-file diffusion for xenon in the nanochannel is persistent even at long diffusion times of over tens of seconds, and found that the observed NMR line shape of xenon within the nanochannels depended on the xenon loading. These results were precisely analyzed by Jameson and de Dios [36], who explained the line shapes in terms of anisotropic averaging of the shielding tensor for xenon atoms in various types of nanochannels, using *ab initio* calculations of ^{129}Xe shielding surfaces. According to the classification of the pore type introduced by Jameson and de Dios, a TPP nanochannel corresponds to a *narrow-bore pipe* model [36].

However, the ^{129}Xe chemical shift will be affected by the existence of helium (He) in the mixture gas, because the density of xenon will change depending on the mixing ratio of He to Xe. Using neat Xe gas, the xenon loading dependence of the chemical shift tensor is expected to accurately provide the information about Xe-wall and Xe-Xe interactions in the channel. The effect of helium on the chemical shift tensor will also be clarified. In addition, the maximum interaction between xenon atoms in the nanochannel will be evaluated from the saturated loading of xenon. Since the ^{129}Xe shielding function between xenon atoms closely depends on the internuclear distance, the maximum interaction will indicate the averaged measurement covering the high-pressure region to the pressure where the adsorption reaches saturation. It will also provide a new insight into the intermolecular interaction relating to the xenon chemical shift as well as the adsorption behavior and local structure of xenon in the nanochannel.

In this study we have carried out high-pressure ^{129}Xe NMR measurements to investigate the pressure dependence of the xenon chemical shift tensor, especially in the pressure region above 0.1 MPa. In addition we examine the relation between the chemical shift and the Xe-wall and the Xe-Xe interactions, in the TPP nanochannel. Furthermore, we attempt to estimate the averaged distance between xenon atoms confined in the nanochannel from the chemical shift difference between the zero loading and saturated loading.

2. Experimental

TPP was synthesized according to the literature [29]. The obtained crude compound was recrystalized from a benzene solution, resulting in a polycrystalline TPP/benzene 1:0.36 inclusion compound (IC). The resultant product was characterized by X-ray powder diffraction [33] and chemical analysis, to confirm the desired compound. The analysis for TPP revealed the following: H: 3.06; C: 49.69; N: 8.56, Calcd.: H: 2.93; C: 49.69; N: 8.62. To produce the guest-free pseudo-hexagonal phase, the powdered sample was heated at 348 K, under reduced pressure (3×10^{-3} kPa) for two hours. Desorption of benzene from the TPP nanochannel was monitored by the weight loss of the sample. The complete desorption of benzene results in a loss of 8.5 % from the initial weight of the sample.

In-situ high-pressure ^{129}Xe NMR measurements were carried out using a Bruker MSL-200 spectrometer operating at a Larmor frequency of 55.678 MHz. A home-built single-tuned pressure-variable NMR probe [11] was used to record the pressure dependence of the ^{129}Xe NMR spectrum confined in the TPP nanochannel. The powdered sample was packed into a glass tube with a dimension of 5 mm ϕ o.d., 3.5 mm ϕ i. d., and 15 mm length; one end rounded. A small amount of glass wool was packed at the open end of the glass tube. This glass tube was then inserted into the zirconia high-pressure cell of the probe [11]. Free induction decay (FID) signals were obtained using a single-pulse sequence. A 90° pulse width of 5 μs and a pulse delay of 2 – 5 s were used. The number of scans varied from 4096 to 24000, depending on the xenon pressure. The ^{129}Xe NMR spectra were recorded at room temperature in the pressure range from 0.02 to 10 MPa. The ^{129}Xe chemical shifts were referred to xenon gas at zero density (δ = 0.0 ppm) [37]. The powder patterns caused by the chemical shift anisotropy were simulated using the WIN-FIT program package supplied by Bruker [38], leading to the components of the chemical shift tensor, $\delta_{\perp}$ and $\delta_{\parallel}$, and the isotropic value of the chemical shift tensor, δ_{iso}.

3. Results and Discussion

3.1. Xe-129 NMR Spectra of Xenon Confined in TPP Nanochannels

Figure 1 shows ^{129}Xe NMR spectra of xenon confined in the TPP nanochannel at room temperature under equilibrium pressures of 1.0 MPa and 0.02 MPa, respectively. The spectrum at 1.0 MPa consists of two peaks; one appears near 0 ppm with 4.0 ppm of full width at half maximum (FWHM), and the other distributes over 36 ppm in the chemical shift range from 121 ppm to 157 ppm. The peak in the vicinity of 0 ppm is attributed to free xenon gas, and the broader one is attributed to xenon confined in the TPP nanochannels based on the chemical shift range. The separation between these signals indicated that the exchange of xenon between the inside and the outside of the channel is slower than about 7 kHz, which corresponds to the frequency separation between the peaks for free Xe gas and xenon confined in the TPP nanochannel. At 0.02 MPa the peak for free Xe gas seems to disappear and only the peak for xenon in the nanochannel is observed. This means that the TPP nanochannel can accommodate xenon below ambient pressure by means of a micropore-filling mechanism, which is caused by the stabilization of xenon due to the dispersion force of the wall in the nanochannel.

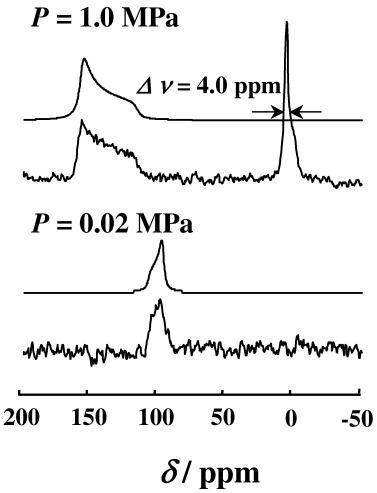

Fig. 1. ^{129}Xe NMR spectra of xenon confined in the TPP nanochannels at 1.0 MPa, and 0.02 MPa. The ^{129}Xe chemical shift is referred to the signal of free xenon gas at zero density.

The line shape of the peak for xenon in the nanochannel exhibits the typical powder pattern that is well-defined by the anisotropy of the chemical shift tensor. In general, the chemical shift tensor is described by three principal values, δ_{11}, δ_{22}, and δ_{33}, where $\delta_{11} \geq \delta_{22} \geq \delta_{33}$. These values lead to meaningful parameters that characterize the shape of the spectrum: the isotropic chemical shift, δ_{iso},

Table 1. ^{129}Xe chemical shift tensor, the isotropic value, the span and the skew for xenon confined in the TPP nanochannel evaluated from the line shape simulation assuming an axially symmetric chemical shift tensor.

P / MPa	$\delta_{\parallel}$ / ppm	$\delta_{\perp}$ / ppm	δ_{iso} / ppm	Ω / ppm	κ / ppm
1.0	121	157	145	36	1
0.02	108	99	102	9	−1

the span, Ω, and the skew, κ. δ_{iso} is given by $(1/3)(\delta_{11}+\delta_{22}+\delta_{33})$, Ω is represented by $\delta_{11}-\delta_{33}$, and κ is given by $3(\delta_{22}-\delta_{\mathrm{iso}})/(\delta_{11}-\delta_{33})$ [39]. In the pseudo-hexagonal lattice of the guest-free TPP crystal, C_3 (or C_6), the symmetry axis passes through the center of the nanochannel along the crystal *c*-axis. This condition requires an axially symmetric chemical shift tensor for xenon in the channel. In this case, the line shape is characterized by only two principal components, $\delta_{\parallel}$ and $\delta_{\perp}$. Here, $\delta_{\parallel}$ is the chemical shift component parallel to the direction of the external field, whereas $\delta_{\perp}$ is the component perpendicular to the external field. The observed line shape seems to be broadened by the axially symmetric chemical shift tensor. The symmetric requirement of the nanochannel leads to the orientation of the principal components of the ^{129}Xe chemical shift tensor of to the channel axis as follows: $\delta_{\parallel}$ lies along the channel axis and $\delta_{\perp}$ is perpendicular to the channel axis. All the principal components at each pressure are evaluated by a line shape simulation, leading to Ω and κ as listed in Table 1. The components of the chemical shift tensor are $\delta_{22}=\delta_{33}=\delta_{\perp}$ and $\delta_{11}=\delta_{\parallel}$, and $\delta_{11}=\delta_{22}=\delta_{\perp}$ and $\delta_{33}=\delta_{\parallel}$ at 0.02 MPa and at 1.0 MPa, respectively. This means that the sign of the skew changes from -1 at 0.02 MPa, to +1 at 1.0 MPa. The change of sign in κ indicates the amount of the xenon loading that affects the shielding components of the chemical shift tensor. This is consistent with the work reported by Sozzani et al. [26, 27], using HP ^{129}Xe NNR with a Xe-He mixture gas at ambient pressure.

The intermolecular shielding for xenon nuclei has been explained by Jameson as a function of molecular configuration with respect to a xenon atom and the interatomic distance [40]. They mentioned that as a partner atom and/or molecule approaches a xenon atom, the partner atom causes a small change in the component of the shielding tensor along the direction coincident with the interatomic vector, whereas it causes large deshielding in the direction perpendicular to the interatomic vector [36]. For xenon confined in the nanochannel, two kinds of collision could be considered – the Xe-wall collision and the Xe-Xe collision. Since the pore diameter of the TPP nanochannel is almost the same size as the van der Waals diameter of xenon, the confined xenon atoms cannot transversely bypass each other in the nanochannel. Therefore $\delta_{\parallel}$ is mainly influenced by the Xe-wall collision interaction, while $\delta_{\perp}$ is mainly influenced by the Xe-Xe collision interaction. As a xenon atom approaches the wall that consists of carbon, hydrogen, nitrogen, and oxygen atoms, the electron cloud of xenon is polarized by these atoms, resulting in more deshielding on the component of the chemical shielding in the direction perpendicular to the Xe-wall axis, $\delta_{\parallel}$. On the other hand, the Xe-Xe collision takes place along the channel axis. The large polarizability of xenon causes large deshielding on the chemical shielding of xenon in the direction perpendicular to the channel axis, $\delta_{\perp}$. According to Jameson, the contribution of the heteroatoms on the wall to the deshielding for xenon-129 is estimated to be only about 10% of the contribution of the xenon atoms [36]. Therefore a much larger deshielding on $\delta_{\perp}$ than $\delta_{\parallel}$ is expected by an increase in the number of collision between xenon atoms.

3.2. Pressure Dependence of the Xe-129 Chemical Shift Tensor in the TPP Nanochannel

Figure 2 shows the pressure dependence of the ^{129}Xe NMR spectrum observed in the pressure range from 0.02 to 10 MPa. The spectrum clearly depends on the Xe loading. The X-ray powder diffraction confirms that even after exposing the TPP sample to a xenon atmosphere at 10 MPa, the crystal did not collapse. With an increase in pressure, the peak for free xenon gas shifts from near 0 ppm at 0.1 MPa to higher frequency, and the peak overlaps with the signal from xenon confined in the nanochannel above 7.0 MPa. This large shift originates by the increase in the density of xenon due to the transition to a supercritical fluid, where the density of xenon reaches approximately 2 g cm^{-3}. On the other hand, for xenon confined in the nanochannel, the span of the powder pattern increases with an increase in pressure. Below 0.03 MPa, $\delta_{\parallel}$ is larger than $\delta_{\perp}$ and κ is -1, whereas in the range of 0.04–0.05 MPa, both components are coalesced and κ becomes zero. This is the first study to observe the pressure dependence of the ^{129}Xe chemical shift tensor confined in the TPP nanochannel, above 0.06 MPa, where κ becomes +1. In addition, it is remarkable that

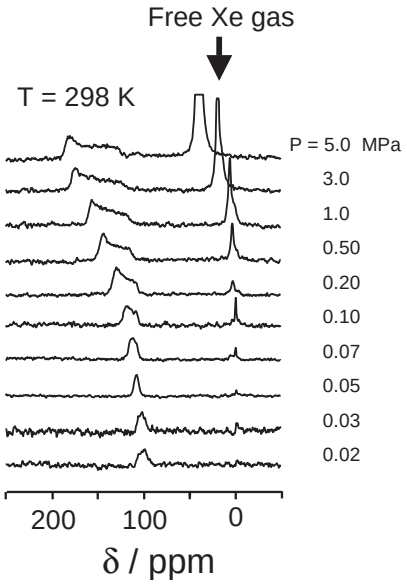

Fig. 2. Pressure dependence of the spectra for xenon in a TPP/Xe system observed from 0.02 – 5 MPa.

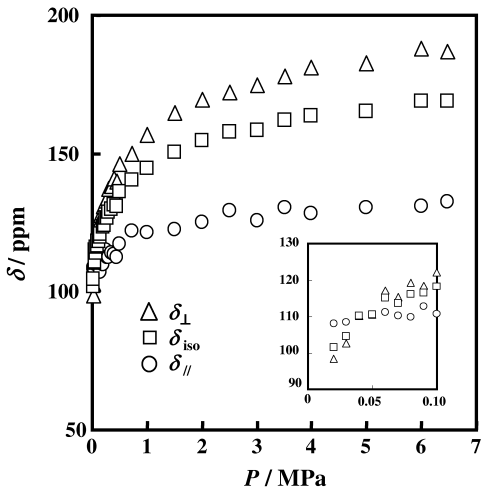

Fig. 3. Pressure dependence of the component of the chemical shift tensor and isotropic value for xenon in the TPP nanochannels from 0.02 to 7 MPa. $\delta_{\|}$ and $\delta_{\perp}$ at each pressure are evaluated from reproducing the line shape by simulation. The inset shows the chemical shift tensor below 0.1 MPa.

$\delta_{\perp}$ becomes larger than $\delta_{\|}$, and the span, Ω, which is the difference between $\delta_{\|}$ and $\delta_{\perp}$, becomes larger as the pressure increases. The components of the chemical shift tensor are evaluated by line shape simulation, with the assumption that the typical powder pattern is broadened by the axially symmetric chemical shift tensor [38]. The pressure dependence of each component of the chemical shift tensor is also shown in Figure 3. $\delta_{\|}$ seems to be constant at all pressures above 0.1 MPa, whereas $\delta_{\perp}$ increases with an increase in pressure. The increase in pressure from 0.02 to 7.0 MPa results in the deshielding of 90 ppm for $\delta_{\perp}$. That is, $\delta_{\perp}$ is mainly attributed to the Xe-Xe collision interactions as described above. In contrast, $\delta_{\|}$ increases by at least 30 ppm, but the increment of $\delta_{\|}$ is much larger than that in AlPO-11 [28] and $(\pm)$-[Co(en)$_3$]Cl$_3$ [15], in which $\delta_{\|}$ changes only slightly after increasing the xenon loading. The pressure dependence of $\delta_{\|}$ implies that the Xe-Xe interaction as well as the Xe-wall interaction should be attributed to $\delta_{\|}$. In a nanochannel with a diameter of 0.45 nm, xenon atoms with the diameter of 0.44 nm can collide with each other on the axis, that is tilted slightly from the channel axis. This off-line collision between xenon atoms in the nanochannel will contribute to the parallel and perpendicular components of the chemical shift tensor.

3.3. Effect of Xe-He Mixture Gas on the Xe-129 Chemical Shift Tensor

Sozzani et al. have observed ^{129}Xe NMR of xenon confined in the TPP nanochannel, using the hyperpolarized xenon in the Xe-He mixture gas under continuous flow condition [26]. They have examined the relation between the chemical shift tensor and the partial pressure of xenon in the mixture gas. In their experiment, the isotropic peak, in which the chemical shift anisotropy apparently disappears, was observed for a xenon concentration of 30 – 50%. This corresponds to 0.03 – 0.05 MPa of the partial pressure of xenon [26]. This pressure range is similar to our result using pure Xe gas under static pressure conditions. However, the ^{129}Xe chemical shift will be affected by the presence of He in the mixture gas, because the density of xenon will change depending on the mixture ratio of He to Xe. In order to clarify the effect of He and the flow condition on the chemical shift tensor, we then examined the pressure dependence of the ^{129}Xe chemical shift tensor in the Xe-He mixture gas under static pressure conditions.

Figure 4 shows the pressure dependence of ^{129}Xe NMR spectra for xenon confined in the nanochannel using pure Xe gas and Xe-He mixture gas, respectively. The pressure of mixture gas was kept constant at 0.1 MPa, and the mixture ratio of He and Xe was varied. The isotropic peak was observed at 0.04 –

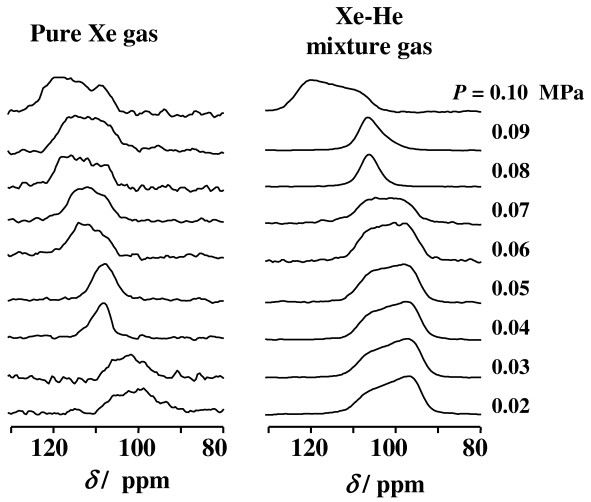

Fig. 4. Xenon loading dependence of ^{129}Xe NMR spectra of xenon confined in TPP nanochannels using pure Xe gas and a Xe-He mixture under static pressure. For pure Xe gas, the representation of pressure shows the true static pressure, whereas for the mixture gas, the partial pressure estimated from the xenon concentration is presented.

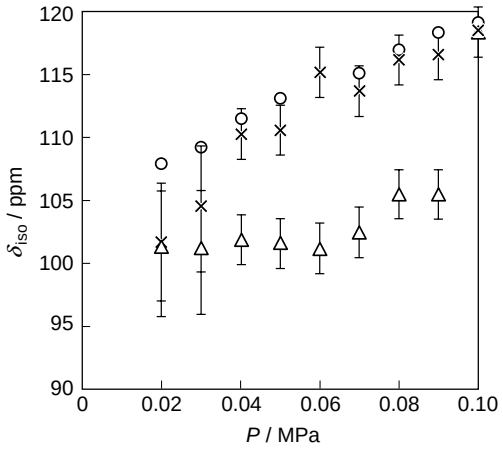

Fig. 5. Pressure dependence of δ_{iso} for pure Xe gas under the static pressure condition ($\times$), for the Xe-He mixture gas under the continuous flow condition ($\circ$), and under the static pressure condition ($\triangle$). δ_{iso} for pure Xe gas under the static pressure condition agrees with the value for the mixture gas under the continuous-flow condition within the experimental error.

0.05 MPa for the pure gas, whereas it was observed at 0.08 – 0.09 MPa for the mixture gas. Since Xe is partially replaced by He in the mixture gas, helium prevents collision between the xenon atoms. The reduction in the number of collisions between the xenon atoms results in lesser deshielding than that in the pure gas. This effect is also reflected in δ_{iso} of the mixture gas under the static pressure conditions as shown in Fig. 5, in which δ_{iso} in the mixture gas becomes smaller than that in the pure Xe gas.

However, δ_{iso} in the Xe-He mixture gas under the continuous-flow condition agrees with our experimental results using the pure Xe gas under static pressure conditions. This may have arisen from a dynamic condition such as the continuous-gas flow. Under the continuous-flow condition, the effect of He on the Xe-Xe collisions may have decreased. In addition, since it is very difficult to control the pressure under the dynamic condition, the chemical shift values in the previous work may accidentally agree with our result observed under the static conditions. Thus, a dynamic condition will lead to complications for the discussion and comparison of the chemical shift values between our result and the previous one obtained under the continuous-flow condition by Sozzani et al. In our experimental set-up it is not necessary to consider the effect of He on the ^{129}Xe chemical shift values, because the Xe-Xe interaction is measured with pressure variation. Therefore, it seems that our results explain the influence of the Xe-Xe interaction for the chemical shift in the TPP nanochannel more clearly than the previous ones.

3.4. The Local Structure of Xe in the TPP Nanochannel

According to Jameson, the ^{129}Xe shielding function caused by the Xe-Xe interaction in a Xe-Xe dimer closely depends on the internuclear distance [40]. The shielding function is concerned with the interatomic potential given by the dispersion force acting between the xenon atoms. Therefore the shielding function exhibits a similar dependence of the interatomic potential on the interatomic distance. For a Xe-Xe distance greater than the equilibrium distance, r_e, at which the Xe dimer has a minimum energy, the ^{129}Xe nuclei are more deshielded with a decrease in the Xe-Xe distance. On the other hand, for a Xe-Xe distance shorter than r_e, the shielding rapidly increases with a decrease in r. If the xenon loading reaches saturation in the TPP nanochannel, the variation in $\delta_{\perp}$ from zero loading to saturation will provide the maximum Xe-Xe in-

teraction for xenon in the TPP nanochannel. The Xe loading is saturated at 6.0 MPa in the TPP nanochannel, at which the average distance between the xenon atoms in the nanochannel becomes minimal. $\delta_\perp$ at zero pressure and at saturated pressure is 98 ppm and 188 ppm, respectively. Calculating the difference between $\delta_\perp$ at zero pressure, $\delta_\perp(0)$, and at saturated pressure, $\delta_\perp$(saturated), an increment of 90 ppm in the chemical shift is found to correspond to maximum Xe-Xe interaction.

According to the additivity of the Xe-Xe interaction contributing to the chemical shielding, as discussed by Jameson and de Dios [36], a contribution of Xe-Xe interaction from a neighboring xenon atom is evaluated to be 45 ppm, because a xenon molecule interacts with two xenon atoms located at both sides of a xenon atom in a one-dimensional nanochannel. This is similar to that for xenon in a large cage of a β-phenol/Xe clathrate compound [36, 41, 42]. In the β-phenol/Xe clathrate compound the Xe-Xe distance is estimated to be 0.53 nm from the diameter of xenon (0.44 nm) and the length of the cage (1.5 nm), at room temperature [41, 42]. The Xe-Xe distance in the TPP nanochannel can also be estimated to equal the interatomic distance in β-phenol/Xe clathrate (0.53 nm).

The *c*-axis of the unit cell of the TPP hexagonal lattice measures 1.008 nm. Therefore, TPP can accommodate up to two xenon atoms in the unit cell, since xenon has a van der Waals diameter of 0.44 nm. The Xe-Xe interatomic distance estimated from $\delta_\perp$ is about half of the *c*-axis of the TPP crystal, and satisfies this requirement of the TPP crystal structure. In addition, the Xe-Xe distance in the TPP nanochannel is also longer than that in solid xenon at 21 K [36, 43]. Solid xenon crystallizes in a face-centered-cubic (fcc) lattice with a = 0.613 nm, leading to a Xe-Xe distance of 0.43 nm [44]. This short Xe-Xe distance means that xenon atoms are tightly bound to each other by the narrow and deep interatomic potential. On the other hand, the larger interatomic distance between xenon atoms in the TPP nanochannel implies that the interatomic interaction between xenon atoms is weaker than that in solid xenon. Thus it is concluded that the interatomic potential for the gaseous state of xenon will be diffused and shallow even in the nanochannel, although the xenon confined in the channel by the micropore filling mechanism is stabilized energetically by the dispersion force from the atoms of the wall.

Conclusion

In-situ high-pressure ^{129}Xe NMR measurement was carried out to examine the pressure dependence of xenon gas in TPP nanochannels. The spectra exhibit a typical powder pattern broadened by the anisotropy of an axially symmetric chemical shift tensor, indicating that the nanochannel is cylindrical. The pressure dependence of $\delta_\perp$ and $\delta_\parallel$ on the axially symmetric chemical shift tensor leads to the orientation of $\delta_\parallel$ and $\delta_\perp$ to the TPP nanochannel axis: $\delta_\parallel$ lies along the channels axis, whereas $\delta_\perp$ is perpendicular to that. Furthermore, this aspect indicates that $\delta_\parallel$ is mainly dominated by Xe-wall collisions, and $\delta_\perp$ is dominated by Xe-Xe collisions. We tried to evaluate the Xe-Xe average distance at saturated loading, using the dependence of Xe-Xe chemical shielding on the internuclear distance. This resulted in a Xe-Xe average distance of 0.54 nm. Thus, this result supports that high-pressure ^{129}Xe NMR is a very useful and powerful tool to explain the local structure of nanochannels and that of the xenon confined in the channel.

[1] J. A. Ripmeester, C. I. Ratcliffe, and J. S. Tse, J. Chem. Soc. Faraday Trans. 1 **84**, 3731 (1988).
[2] J. A. Ripmeester and C. I. Ratcliffe, J. Phys. Chem. **94**, 8773 (1990).
[3] P. J. Barrie and J. Klinowski, Prog. NMR Spectrosc. **24**, 91 (1992).
[4] D. Raftery and B. F. Chmelka, NMR **30**, 112 (1994).
[5] J. M. Kneller, R. J. Soto, S. E. Surber, J.-F. Colomer, A. Fonseca, J. B. Nagy, G. V. Tendeloo, and T. Pietrass, J. Amer. Chem. Soc. **122**, 10591 (2000).
[6] J. A. Ripmeester and C. I. Ratcliffe, J. Phys. Chem. **94**, 7652 (1990).
[7] I. L. Moudrakovski, V. V. Terskikh, C. I. Ratcliffe, J. A. Ripmeester, L.-Q. Wang, Y. Shin, and G. J. Exarhos, J. Phys. Chem. B **106**, 5938 (2002).
[8] I. L. Moudrakovski, A. Sanchez, C. I. Ratcliffe, and J. A. Ripmeester, J. Phys. Chem. B **104**, 7306 (2000).
[9] M. S. Syamala, R. J. Cross, and M. Saunders, J. Amer. Chem. Soc. **124**, 6216 (2002).
[10] M. Tomaselli, B. H. Meier, P. Robyr, U. W. Suter, and R. R. Ernst, Chem. Phys. Lett. **205**, 145 (1993).
[11] B. Nagasaka, H. Omi, T. Eguchi, H. Nakayama, and N. Nakamura, Chem. Phys. Lett. **340**, 473 (2001).
[12] J. Demarquay and J. Fraissard, Chem. Phys. Lett. **136**, 314 (1987).
[13] I. L. Moudrakovski, A. A. Sanchez, C. I. Ratcliffe, and J. A. Ripmeester, J. Phys. Chem. B **105**, 12338 (2001).
[14] T. T. P. Cheung, J. Phys. Chem. **99**, 7089 (1995).

[15] T. Ueda, T. Eguchi, N. Nakamura, and R. E. Wasylishen, J. Phys. Chem. B **107**, 180 (2003).
[16] T. Pietrass, Magn. Reson. Rev. **17**, 263 (2000).
[17] B. M. Goodson, J. Magn. Reson. **155**, 157 (2002).
[18] C. R. Bowers, H. W. Long, T. Pietrass, H. C. Gaede, and A. Pines, Chem. Phys. Lett. **205**, 168 (1993).
[19] H. W. Long, H. C. Gaede, J. Shore, L. Reven, C. R. Bowers, J. Kritzenberger, T. Pietrass, and A. Pines, J. Amer. Chem. Soc. **115**, 8491 (1993).
[20] E. Brunner, M. Haake, A. Pines, J. A. Reimer, and R. Seydoux, Chem. Phys. Lett. **290**, 112 (1998).
[21] T. Rõõm, S. Appelt, and R. Seydoux, Phys. Rev. **B 55**, 11604 (1997).
[22] E. MacNamara, G. Fisher, J. Smith, C. V. Rice, S.-J. Hwang, and D. Raftery, J. Phys. Chem. B **103**, 1158 (1999).
[23] C. R. Bowers, V. Storhaug, C. E. Webster, J. Bharatam, A. Cottone III, R. Gianna, K. Betsey, and B. J. Gaffney, J. Amer. Chem. Soc. **121**, 9370 (1999).
[24] V. V. Terskikh, I. L. Moudrakovski, H. Du, C. I. Ratcliffe, and J. A. Ripmeester, J. Amer. Chem. Soc. **123**, 10399 (2001).
[25] S. Appelt, F. W. Haesing, S. Baer-Lang, N. J. Shah, and B. Blümich, Chem. Phys. Lett. **348**, 263 (2001).
[26] P. Sozzani, A. Comotti, R. Simonutti, T. Meersmann, J. W. Logan, and A. Pines, Angew. Chem. Int. Ed. **39**, 2695 (2000).
[27] T. Meersmann, J. W. Logan, R. Simonutti, S. Caldarelli, A. Comotti, P. Sozzani, L. G. Kaiser, and A. Pines, J. Phys. Chem. A **2**, 11665 (2000).
[28] J. A. Ripmeester and C. I. Ratcliffe, J. Phys. Chem. **99**, 619 (1995).
[29] H. R. Allcock, J. Amer. Chem. Soc. **86**, 2591 (1964).
[30] H. R. Allcock and L. A. Siegel, J. Amer. Chem. Soc. **86**, 5140 (1964).
[31] H. R. Allcock, Chem. Rev. **72**, 315 (1972).
[32] A. Comotti, R. Simonutti, S. Stramare, and P. Sozzani, Nanotechnology **10**, 70 (1999).
[33] L. A. Siegel and J. H. van den Hende, J. Chem. Soc. **A**, 817 (1967).
[34] E. Meirovitch, I. Belsky, and S. Vega, J. Phys. Chem. **88**, 1522 (1984).
[35] E. Meirovitch, J. Phys. Chem. **88**, 6411 (1984).
[36] C. J. Jameson and A. C. de Dios, J. Chem. Phys. **116**, 3805 (2002).
[37] A. K. Jameson, C. J. Jameson, and H. S. Gutowsky, J. Chem. Phys. **53**, 2310 (1970).
[38] This program was supplied by Bruker Franzen Analytik GmbH And S. A. D. I. S. Bruker Spectrospin.
[39] J. Mason, J. Solid State Nucl. Magn. Reson. **2**, 285 (1993).
[40] C. J. Jameson and A. C. de Dios, J. Chem. Phys. **97**, 417 (1992).
[41] J. A. Ripmeester, J. Amer. Chem. Soc. **104**, 289 (1982).
[42] M. Von Stackelberg, A. Hoverath, and C. Scheringer, Z. Elektrochem. **62**, 123 (1958).
[43] D. Brinkmann and H. Y. Carr, Phys. Rev. **150**, 174 (1966).
[44] D. R. Sears and H. P. Klug, J. Chem. Phys. **37**, 3002 (1962).